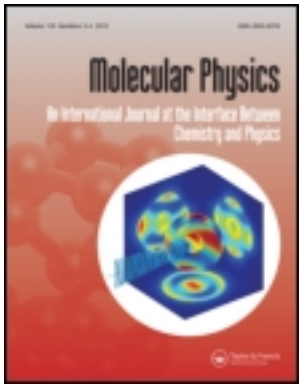

Molecular Physics: An International Journal at the Interface Between Chemistry and Physics
Publication details, including instructions for authors and subscription information:
http://www.tandfonline.com/loi/tmph20

Structure, thermodynamic and transport properties of imidazolium-based bis(trifluoromethylsulfonyl)imide ionic liquids from molecular dynamics simulations

Eleni Androulaki [a] , Niki Vergadou [a] , Javier Ramos [b] & Ioannis G. Economou [a c]

[a] National Center for Scientific Research "Demokritos", Institute of Physical Chemistry, Molecular Thermodynamics and Modelling of Materials Laboratory, GR-153 10, Aghia Paraskevi Attikis, Greece

[b] Department of Macromolecular Physics, Instituto de Estructura de la Materia - CSIC, Serrano 113bis, ES-28006 Madrid, Spain

[c] The Petroleum Institute, Department of Chemical Engineering, PO Box 2533, Abu Dhabi, United Arab Emirates

Accepted author version posted online: 01 Mar 2012.Version of record first published: 11 Apr 2012.

To cite this article: Eleni Androulaki, Niki Vergadou, Javier Ramos & Ioannis G. Economou (2012): Structure, thermodynamic and transport properties of imidazolium-based bis(trifluoromethylsulfonyl)imide ionic liquids from molecular dynamics simulations, Molecular Physics: An International Journal at the Interface Between Chemistry and Physics, 110:11-12, 1139-1152

To link to this article: http://dx.doi.org/10.1080/00268976.2012.670280

Molecular Physics
Vol. 110, Nos. 11–12, 10–20 June 2012, 1139–1152

Taylor & Francis
Taylor & Francis Group

INVITED ARTICLE

Structure, thermodynamic and transport properties of imidazolium-based bis(trifluoromethylsulfonyl)imide ionic liquids from molecular dynamics simulations

Eleni Androulaki[a], Niki Vergadou[a], Javier Ramos[b] and Ioannis G. Economou[ac]*

[a]*National Center for Scientific Research "Demokritos", Institute of Physical Chemistry, Molecular Thermodynamics and Modelling of Materials Laboratory, GR-153 10, Aghia Paraskevi Attikis, Greece;* [b]*Department of Macromolecular Physics, Instituto de Estructura de la Materia – CSIC, Serrano 113bis, ES-28006 Madrid, Spain;* [c]*The Petroleum Institute, Department of Chemical Engineering, PO Box 2533, Abu Dhabi, United Arab Emirates*

(*Received 18 November 2011; final version received 22 February 2012*)

Molecular dynamics (MD) simulations have been performed in order to investigate the properties of $[C_n mim^+][Tf_2N^-]$ ($n = 4, 8, 12$) ionic liquids (ILs) in a wide temperature range (298.15–498.15 K) and at atmospheric pressure (1 bar). A previously developed methodology for the calculation of the charge distribution that incorporates *ab initio* quantum mechanical calculations based on density functional theory (DFT) was used to calculate the partial charges for the classical molecular simulations. The wide range of time scales that characterize the segmental dynamics of these ILs, especially at low temperatures, required very long MD simulations, on the order of several tens of nanoseconds, to calculate the thermodynamic (density, thermal expansion, isothermal compressibility), structural (radial distribution functions between the centers of mass of ions and between individual sites, radial-angular distribution functions) and dynamic (relaxation times of the reorientation of the bonds and the torsion angles, self-diffusion coefficients, shear viscosity) properties. The influence of the temperature and the cation's alkyl chain length on the above-mentioned properties was thoroughly investigated. The calculated thermodynamic (primary and derivative) and structural properties are in good agreement with the experimental data, while the extremely sluggish dynamics of the ILs under study renders the calculation of their transport properties a very complicated and challenging task, especially at low temperatures.

Keywords: ionic liquids; imidazolium; molecular simulation; physical properties

1. Introduction

Ionic liquids (ILs) refer to salts that are in the liquid phase at room temperature and, by convention, below 100°C [1,2]. They usually consist of a wide range of anions (halides, inorganic or large organic anions) and multi-atomic and asymmetric organic cations, thereby leading to lower melting temperatures than ordinary salts. In recent years, ILs have attracted increasing interest for extended study aiming at their potential use in a broad range of applications due to their unique combination of a number of properties. One of their most important attributes is their negligible vapor pressure, which results in minimal vapor emissions that makes them odorless, non-flammable and, therefore, excellent candidates for use in 'green chemistry' as environmentally friendly materials. Other notable properties that have been reported are their ability to dissolve a number of organic and inorganic substances, the high thermal and electrochemical stability, the wide temperature range at which they are in the liquid phase, as well as good lubricant properties. The combination of these properties makes them suitable for a number of industrial applications, for instance as solvents and catalysts in chemical synthesis, as lubricants in tribology applications, as electrolytes in electrochemistry and in gas storage and separation applications [2–8].

The very large number of anions and cations that can be combined leads to a plethora of ILs that can be synthesized. The chemical diversity in the molecular structure of the ions involved affects directly the physicochemical properties of the ILs, thus enabling the tuning [3,9–12] of the properties of an IL by making moderate changes to the ions' chemical formula and structure. A large number of experimental investigations [9,10,13–41] have been conducted in order to measure a wide range of IL properties (volumetric, thermal, transport, etc.), while molecular

*Corresponding author. Email: economou@chem.demokritos.gr

ISSN 0026–8976 print/ISSN 1362–3028 online

http://dx.doi.org/10.1080/00268976.2012.670280
http://www.tandfonline.com

simulation [42–53] has been widely used to study the underlying molecular mechanisms that govern the macroscopic properties of these physical systems by giving insight into the microscopic behavior that controls the experimentally observed phenomena. The vast majority of the molecular simulation studies have used all-atom force fields incorporating *ab initio* parameterization of single ions in the gas phase. Coarse-grained models have also been used to accelerate calculations and to access longer length- and time-scales for the study of IL systems [54,55], whereas lately the role of polarizability has been under investigation [53,56,57].

In the present work, ILs from the bis(trifluoromethylsulfonyl) imide ($[Tf_2N^-]$) family with *n*-alkyl methyl imidazolium-based cations ($[C_nmim^+]$) are studied. These ILs have received significant attention both experimentally and computationally using molecular simulation due to the fact that $[Tf_2N^-]$ has been selected by the International Union of Pure and Applied Chemistry (IUPAC) as a benchmark anion in ILs for extensive investigation. More specifically, the $[C_nmim^+][Tf_2N^-]$ ($n = 4, 8, 12$) ILs are examined in a wide range of temperatures by means of molecular dynamics (MD) simulation. This type of cation consists of an imidazolium ring and, in our case, one alkyl chain with *n* carbon atoms. This work focuses on elucidating the influence of the alkyl chain length on the IL thermodynamic, structural and transport properties. Moreover, the temperature effect on the properties under study is thoroughly investigated in order to examine the behavior of each IL under high temperature conditions where no experimental data exist.

The structure of the paper is as follows. Section 2 reports the simulation details and the force field used. In Section 3 the results are presented for the thermodynamic (density, thermal expansion, isothermal compressibility), structural (radial distribution functions between the centers of mass of ions and radial distribution functions between different sites of the ions, radial-angular distribution functions, end-to-end distance distributions), segmental dynamic and transport (self-diffusion coefficients, shear viscosity) properties of the three ILs, $[C_4mim^+][Tf_2N^-]$, $[C_8mim^+][Tf_2N^-]$ and $[C_{12}mim^+][Tf_2N^-]$, under study. Conclusions are given in Section 4.

2. Methodology

2.1. *Simulation details*

Long MD simulations were performed in different thermodynamic ensembles at temperatures ranging from 298.15 to 498.15 K in 50 K increments and 1 bar pressure using NAMD [58]. Each system consisted of 100 $[C_nmim^+][Tf_2N^-]$ ($n = 4, 8, 12$) ion pairs which were initially placed in a simulation box according to a target density. The value of the initial density used for each system was extracted from the experimental data, either directly when available, as for the case of $[C_4mim^+][Tf_2N^-]$ and $[C_8mim^+][Tf_2N^-]$ at 298.15 K [10,13], or indirectly by interpolating and/or extrapolating the available data at various temperatures. For the case of $[C_{12}mim^+][Tf_2N^-]$ where no experimental data were found in the literature, a different approach was followed: first, all the experimental data for smaller alkyl chain lengths [9,10,13,17–39] were gathered and for each alkyl chain length the values of the density at all temperatures under study were determined by extrapolating or interpolating the available experimental data. Then, for each specific temperature under consideration the target density for $[C_{12}mim^+][Tf_2N^-]$ was calculated by extrapolating the existing data for smaller alkyl chain lengths. The initial structures were built using the Rotational Isomeric State (RIS) model [59] as modified by Theodorou and Suter [60,61] available in MAPS [62]. Then, a 10^5 steps conjugate gradient energy minimization procedure was applied to eliminate the atomic overlaps and a 5 ns simulation in the canonical ensemble (NVT) was conducted in order to equilibrate the system. Subsequently, simulations in the isobaric–isothermal ensemble (NPT) on the order of 25–60 ns, depending on the system, were carried out to further equilibrate the system and the thermodynamic properties relevant to this ensemble were calculated using the last 15–30 ns of the NPT runs, having first adequately equilibrated the system. Next, a 10–20 ns NVT simulation was carried out in order to calculate the dynamic and structural properties of the system. Snapshots were stored every 1 ps during each simulation. A Langevin piston method was used for the temperature control with a $5\,ps^{-1}$ damping factor, while the Nosé–Hoover barostat was used for the pressure control with oscillation period equal to 200 fs and damping factor 100 fs. Electrostatics were handled by means of the particle-mesh Ewald method while the reversible reference system propagator algorithm (rRESPA) [63,64] was used as a multiple time step algorithm with a 1 fs reference time step in order to speed up the MD simulations. Short-range non-bonded van der Waals interactions were calculated every 2 fs, while full electrostatic interactions were computed every 4 fs. A cutoff distance of 12 Å was used to truncate the van der Waals interactions.

2.2. *Force field*

The all-atom force field used to model the potential energy of the ILs under investigation is based on the following expression:

$$U = \sum_{bonds} k_b(b-b_0)^2 + \sum_{angles} k_\theta(\theta-\theta_0)^2 + \sum_{dihedrals}\sum_{n=1}^{4} k_\chi[1+\cos(n\chi-\delta)] + \sum_{impropers} k_\psi(\psi-\psi_0)^2 + \sum_{i=1}^{n-1}\sum_{j>i}^{n}\left\{4\varepsilon_{ij}\left[\left(\frac{\sigma_{ij}}{r_{ij}}\right)^{12}-\left(\frac{\sigma_{ij}}{r_{ij}}\right)^{6}\right]+\frac{q_iq_j}{4\varepsilon_0 r_{ij}}\right\}, \quad (1)$$

where b, θ, χ and ψ denote bond length, bond angle, dihedral angle and improper angle, respectively, and the subscript '0' refers to the equilibrium values. Parameter n in the expression for the dihedral potential is the multiplicity of the dihedral angle while δ is the phase shift of the dihedral potential over the full range of rotation. Partial charges are denoted by q_i, while ε_0 is the vacuum permittivity and ε and σ the Lennard–Jones parameters. Bonded and Lennard–Jones parameters were obtained from Cadena and Maginn [65] and from Cadena *et al*. [66] for the cations and Canongia Lopes and Pádua [67] for the anion. The partial charges were derived from quantum calculations performed on an isolated $[C_n mim^+][Tf_2N^-]$ ($n=4, 8, 12$) ion pair using a Density Functional Theory (DFT) methodology [43] according to which the atomic charges were calculated by taking into account the relative position and orientation of the anion with respect to the cation. For that, six minimum energy configurations of the ionic pair were used and the atomic charges at the different ionic pair conformations were calculated by electrostatic surface potential fits. Subsequently, the mean value of each atomic charge from the six different distributions was calculated and assigned to the atoms. A Boltzmann weighted scheme based on the energy of each minimum energy configuration was also investigated for the calculation of the partial charges with no apparent influence on the systems' thermodynamic and structural properties and was, therefore, not used subsequently. An additional modification to the charges of the anion's atoms was applied in order to preserve the symmetry of the anion by assigning to each group of symmetric atoms the mean value of the charges estimated by the quantum mechanical calculations. All force field parameters are provided as supplementary material.

3. Results and discussion

In this section the results for the thermodynamic, structural and transport properties as calculated from the MD simulations are presented. The chemical structure of the three ILs ions and the labeling of their atoms are shown in Figure 1.

3.1. *Thermodynamic properties*

Table 1 presents the MD calculations for the mass density of the three ILs. Density calculations from the NPT MD simulations resulted in less than 2% deviation from the available experimental measurements [10,13,16], which are limited to 288.15–328.20 K for the cases of $[C_4mim^+][Tf_2N^-]$ and $[C_8mim^+][Tf_2N^-]$. For a given temperature, the density decreases as the length of the alkyl chain in the cation increases.

Furthermore, MD data were used to calculate the isobaric thermal expansion coefficient, a_p, given by the expression

$$a_p = \frac{1}{V}\left(\frac{\partial V}{\partial T}\right)_p = \frac{1}{\langle V\rangle}\left(\frac{\Delta\langle V\rangle}{\Delta T}\right)_P = \frac{\langle \delta V \delta H\rangle_{NPT}}{\langle V\rangle k_B T^2}, \quad (2)$$

as well as the isothermal compressibility, k_T, through the expression

$$k_T = -\frac{1}{V}\left(\frac{\partial V}{\partial P}\right)_T = -\frac{1}{\langle V\rangle}\left(\frac{\Delta\langle V\rangle}{\Delta P}\right)_T. \quad (3)$$

Tables 2 and 3 show the estimated values of a_p and k_T for all ILs. They exhibit less than 15% deviation, on average, from the available experimental data [13] for $[C_4mim^+][Tf_2N^-]$. No data were available in the literature for $[C_8mim^+][Tf_2N^-]$ and $[C_{12}mim^+][Tf_2N^-]$.

3.2. *Microscopic structure*

The ions' organization in space was examined by means of radial distribution functions (RDFs) between the ions' centers-of-mass as well as between specific atoms in the ions. Further insight into the conformations of the alkyl chain was generated by the calculation of the end-to-end distance distribution for the cation's alkyl chain. Figure 2 shows the RDFs of the center-of-mass for anion–anion, cation–cation and cation–anion interactions for $[C_8mim^+][Tf_2N^-]$ at 398.15 K and 1 bar. The anion–anion RDF exhibits a first peak at approximately 8 Å with a second, less intense peak appearing at 17 Å. The cation–anion RDF has a first maximum at around 5 Å and a second one, less intense at 12.5 Å, while the cation–cation RDF exhibits one small but broad maximum at 10 Å. Comparison of the three RDFs reveals a stronger

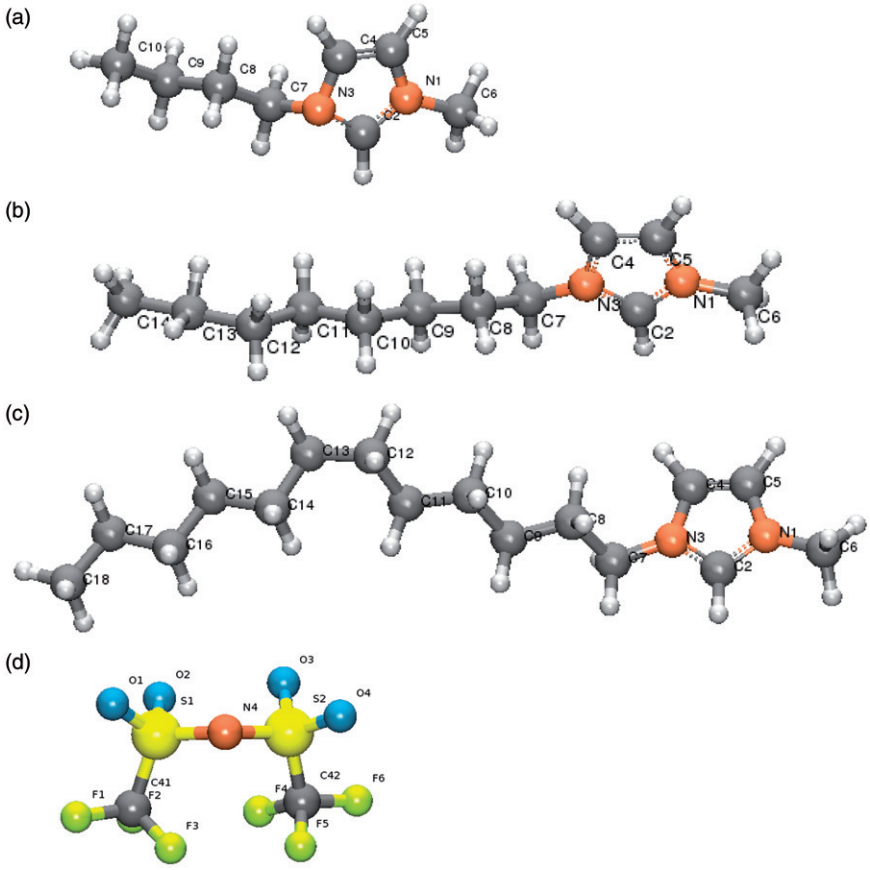

Figure 1. Ions (a) $[C_4mim^+]$, (b) $[C_8mim^+]$, (c) $[C_{12}mim^+]$ and (d) $[Tf_2N^-]$ and labelling of the atoms.

Table 1. Mass density calculations for the three ILs at different temperatures and 1 bar. In all cases, the statistical uncertainty is less than 0.001.

	Mass density ($g\,cm^{-3}$)		
T (K)	$[C_4mim^+][Tf_2N^-]$	$[C_8mim^+][Tf_2N^-]$	$[C_{12}mim^+][Tf_2N^-]$
298.15	1.461	1.331	1.250
348.15	1.406	1.278	1.205
398.15	1.354	1.228	1.158
448.15	1.303	1.180	1.113
498.15	1.252	1.131	1.068

Table 2. Thermal expansion coefficient, a_p, for the three ILs at different temperatures and 1 bar.

	a_p (10^{-4}/K)		
T (K)	$[C_4mim^+][Tf_2N^-]$	$[C_8mim^+][Tf_2N^-]$	$[C_{12}mim^+][Tf_2N^-]$
298.15	7.4_1	7.2_9	7.02_1
348.15	8.9_8	8.48_9	8.2_8
398.15	7.5_3	8.8_5	8.5_4
448.15	7.9_3	8.2_5	8.9_7
498.15	8.1_1	9.9_6	9.2_1

cation–anion interaction due to the ions' opposite charges, whereas the ions clearly retain their spatial organization at longer distances compared with ordinary molecular liquids. This behaviour has been reported for a number of ILs as well as in both experimental [14,68–70] and simulation studies [44,65,66,71–74] and is also observed for $[C_4mim^+][Tf_2N^-]$, but becomes less evident in the case of $[C_{12}mim^+][Tf_2N^-]$ for the anion–cation interaction, a fact that can be attributed to the existence of additional neutral parts in the system as the alkyl tail becomes longer. As shown in Figure 3, a drop in the value of the first maximum of the cation–anion RDF is observed while the second and less intense maximum tends to disappear as the alkyl chain becomes longer. Additionally, a longer alkyl chain causes greater

Table 3. Isothermal compressibility, k_T, for the three ILs at different temperatures and 1 bar.

	k_T (10^{-4}/MPa)		
T (K)	[C_4mim$^+$][Tf_2N^-]	[C_8mim$^+$][Tf_2N^-]	[C_{12}mim$^+$][Tf_2N^-]
298.15	4.7_6	4.54_7	4.5_4
348.15	5.9_4	6.3_3	6.5_4
398.15	7.4_3	7.9_3	8.3_3
448.15	9.6_4	9.9_3	10.7_2
498.15	12.3_3	14.1_4	13.6_3

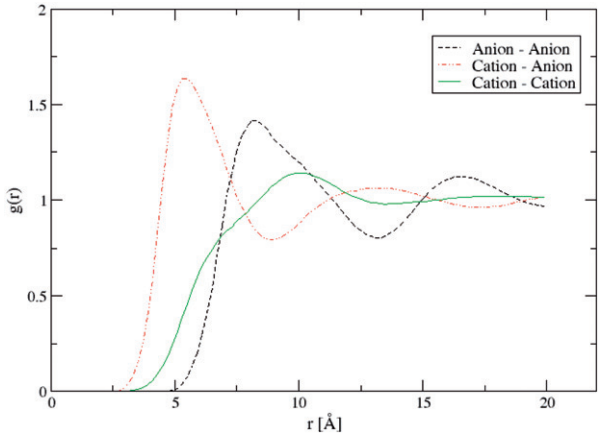

Figure 2. Radial distribution function $g(r)$ for the anion–anion (black), anion–cation (red) and cation–cation (green) center of mass of [C_8mim$^+$][Tf_2N^-] at 398.15 K and 1 bar.

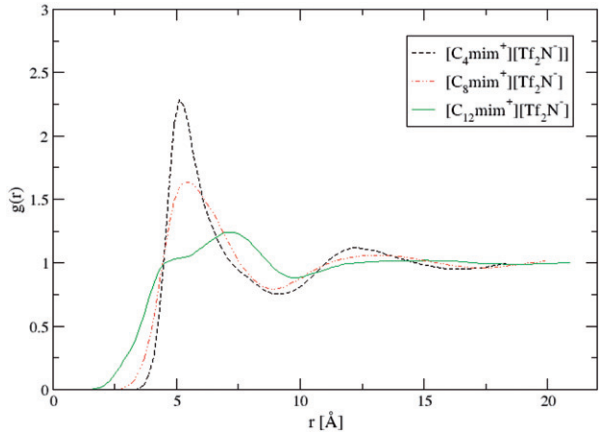

Figure 3. Radial distribution function $g(r)$ for the cation–anion centers of mass of [C_4mim$^+$][Tf_2N^-], [C_8mim$^+$][Tf_2N^-] and [C_{12}mim$^+$][Tf_2N^-] at 398.15 K and 1 bar.

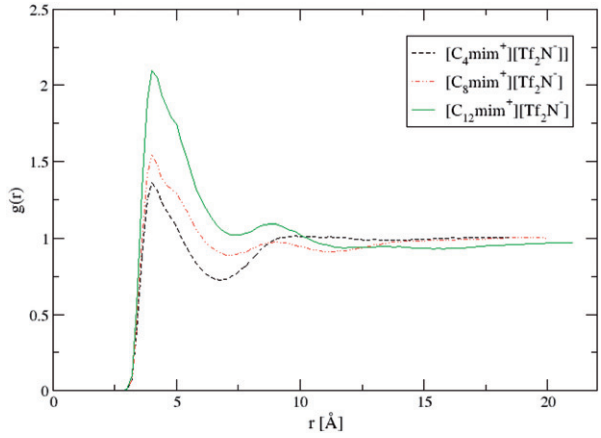

Figure 4. Radial distribution function $g(r)$ between the terminal carbon atoms in the cation's alkyl chain of [C_4mim$^+$][Tf_2N^-], [C_8mim$^+$][Tf_2N^-] and [C_{12}mim$^+$][Tf_2N^-] at 398.15 K and 1 bar.

delocalization of the cation's center of mass and an increase in the distance where the maximum value appears. Raising the temperature does not significantly affect the RDFs between the ions' centers of mass, apart from 298.15 K where some characteristics of the RDFs are more pronounced.

A more detailed insight into the liquid bulk structure can be obtained from RDFs between specific sites of the ions. Figure 4 shows the RDFs between the terminal carbon atoms of the alkyl chain for each IL at 398.15 K and 1 bar. For all ILs there is a first peak at approximately 4.5 Å and a second one that starts to appear at around 8.5 Å as the alkyl chain becomes longer. The temperature increase resulted in a clear drop in the value of the first maximum while the second was less affected. Interestingly, the intensity of the first peak increases as the alkyl chain becomes longer, although it always appears at almost the same distance. This indicates that the almost neutrally charged and non-polar alkyl chains tend to aggregate and form domains while the charged groups of the cations and the anions create a charged network by retaining their structures up to long distances, a trend that has been reported in previous studies [42,43,49–52]. A possible mechanism that explains this behaviour has been suggested by Wang *et al.* [52] and is based on the existence of competitive electrostatic and van der Waals interactions in the ILs that dominate different parts of the ILs. For the charged parts of the system, i.e. the imidazolium ring and the anion, the electrostatic interactions dominate their local behaviour while the short-ranged van der Waals interactions become significant when these groups come very close. Electrostatic interactions are

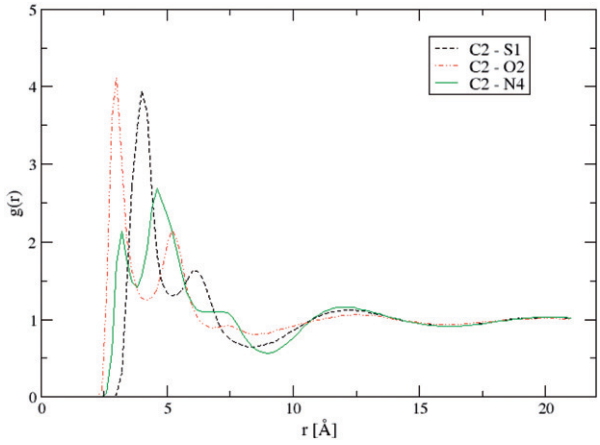

Figure 5. Radial distribution function $g(r)$ between the C_2 carbon in the imidazolium ring and S1, O2 and N4 in the anion of $[C_{12}mim^+][Tf_2N^-]$ at 398.15 K and 1 bar.

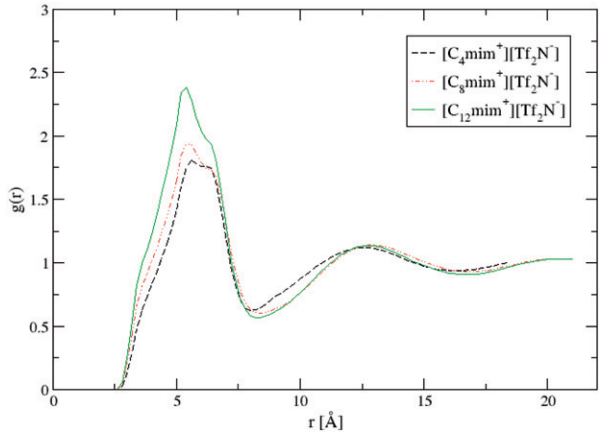

Figure 6. Radial distribution function $g(r)$ between C4 of the imidazolium ring and N4 of the anion of $[C_4mim^+][Tf_2N^-]$, $[C_8mim^+][Tf_2N^-]$ and $[C_{12}mim^+][Tf_2N^-]$ at 398.15 K and 1 bar.

long-ranged and strong, so the charged groups retain their local structures and form continuous charged domains. On the other hand, in the non-polar regions of the ILs, i.e. the almost neutral alkyl chain, the short-ranged van der Waals interactions are dominant, thus leading to tail aggregation phenomena.

More information on the relative configurations of the polar groups, i.e. the anions and the imidazolium rings, can be obtained by the RDFs between specific atoms in these groups. The RDFs between the carbon atoms C2 and C4 on the imidazolium and the atoms S1, O2 and N4 of the anion were calculated. Figure 5 shows the RDFs between the C2 carbon on the imidazolium ring and S1, O2 and N4 of the anion of $[C_{12}mim^+][Tf_2N^-]$ at 398.15 K and 1 bar. The C2–O2 RDF has a first peak at around 2.5 Å and a less intense one at around 5 Å. Since O2 is covalently bonded to S1 with a double bond, the RDF between C2 and S1 is of similar form to that of the C2–O2 pair with the first peak appearing at a slightly longer distance (4 Å) and the second one much less intense at approximately 6.5 Å. The RDF between C2 and N4 indicates that, at small distances, where O2 or S1 is most likely to be found close to the C2 carbon atom, N4 can be found anywhere between 3 and 6 Å as the value of the RDF at these distances is greater than one. Nevertheless, the two peaks show that there are preferential relative positions and the first peak at 3 Å may be indicative of a configuration where the N4 nitrogen of the anion comes close to the C2 carbon atom on the imidazolium ring, while the second and more intense peak may correspond to the most probable case where the O2 and S1 atoms are closer to the C2 carbon. The nitrogen N4, which is covalently bonded to S1, is most likely to be found at a slightly longer distance. The RDFs between C4 and the O2, S1, N4 of the anion at all ILs highlight this preferential conformation between C2 and the above anion atoms. An example of such RDFs is shown in Figure 6, which shows the RDFs between the C4 on the imidazolium ring and the N4 of the anion of $[C_4mim^+][Tf_2N^-]$, $[C_8mim^+][Tf_2N^-]$ and $[C_{12}mim^+][Tf_2N^-]$ at 398.15 K and 1 bar. For all ILs there is one peak that appears at approximately 5 Å and becomes more intense as the alkyl chain length increases.

Additional details on the microscopic structure of ILs can be obtained from the calculation of three-dimensional radial-angular distribution functions (RADF). Figure 7 compares the RADFs between the C2 carbon atom of the imidazolium ring and the N4 nitrogen of the anion for the three ILs. The angle θ is the angle formed by the main plain of the imidazolium ring and the vector that connects the C2 and N4 atoms. In all cases, the main peaks appear at about 4–5 Å and at symmetrical positions above and below the plain of the imidazolium ring. A second peak is also observed at around 7–8 Å and at 0° angle for all ILs. Extra RADFs calculated (not shown here) measuring the distance between the geometrical center of the imidazolium ring and the N4 nitrogen of the anion indicate that this second peak corresponds to the case where the N4 nitrogen of the anion lies on the plane of the imidazolium ring but is situated not close to the C2 carbon atom but on the other side of the imidazolium ring, that is closer to the C4 and C5 carbon atoms. For the case of the longest alkyl chain, i.e. the $[C_{12}mim^+][Tf_2N^-]$ IL, there is also a third peak appearing at shorter distances, at about 3 Å, whereas

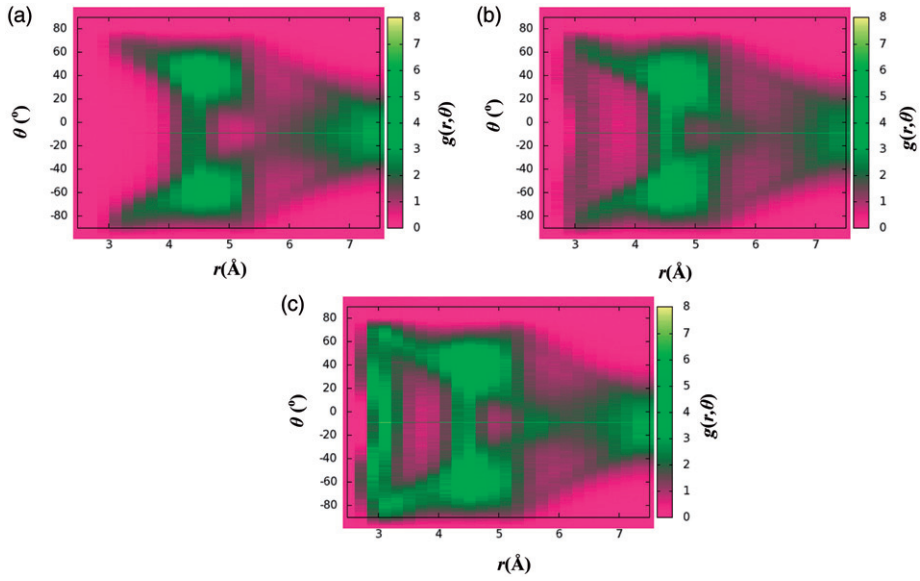

Figure 7. Radial angular distribution functions (RADF) for (a) $[C_4mim^+][Tf_2N^-]$, (b) $[C_8mim^+][Tf_2N^-]$ and (c) $[C_{12}mim^+][Tf_2N^-]$ at 298.15 K with r being the distance between the C2 carbon atom of the imidazolium ring and the N4 nitrogen atom of the anion and θ is the angle formed by the main plain of the imidazolium ring and the vector **r**.

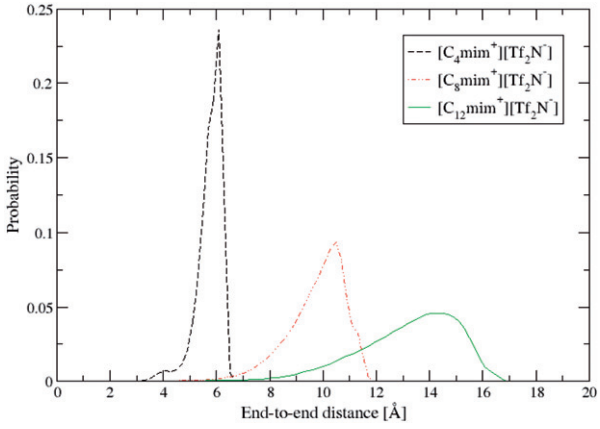

Figure 8. Alkyl chain end-to-end distance distribution of $[C_4mim^+][Tf_2N^-]$, $[C_8mim^+][Tf_2N^-]$ and $[C_{12}mim^+][Tf_2N^-]$ at 398.15 K and 1 bar.

it spans over almost the whole range of the angles. This is consistent with the results obtained from the RDFs between the terminal carbon atoms in the alkyl chain, where the longest alkyl chain had the most intense peak in the RDF (Figure 4). These two findings clearly suggest that, as the alkyl chain becomes longer, not only do the alkyl tail groups come closer, but also the anion approaches the imidazolium ring and, more precisely, the C2 carbon atom. Generally, a temperature increase resulted in a slight decrease in the maximum values of all atom–atom RDFs and RADFs studied with no particular change to the overall spatial organization of the ions.

Insight into the cation's alkyl chain conformations can be obtained from the calculation of the distribution of the end-to-end distance for all ILs. The end-to-end distance, R_e, was chosen to be calculated as the distance between the geometrical center of the imidazolium ring and the terminal carbon atom of the alkyl chain of each IL. Figure 8 shows the distribution of the end-to-end distance for each IL at 398.15 K and 1 bar. The end-to-end distance distribution is a right-shifted normal distribution for each IL, with the variance around the mean value becoming higher as the alkyl chain becomes longer, indicating that a longer alkyl chain is more flexible. A temperature increase systematically decreases the mean value of the end-to-end distance and increases the variance around the mean value. These data were fit to the expression

$$\langle R_e^2 \rangle \propto N^{2\nu}, \tag{4}$$

where N is the number of carbon atoms of the alkyl chain and ν was found equal to 0.74, 0.76 and 0.8 for $T = 298.15$, 398.15 and 498.15 K, respectively, being in very good agreement with simulation calculations on low-molecular-weight alkanes [75,76].

3.3. *Local dynamics*

The local dynamics of each of the systems was examined through the decorrelation of the orientation of various vectors defined by atoms on the ions as well as through torsion angle decorrelation.

The reorientation of vectors is quantified by a second-order autocorrelation function of the form

$$P_2(t) = \frac{1}{2}\left\{3\left\langle[\mathbf{u}_{CH}(t)\cdot\mathbf{u}_{CH}(0)]^2\right\rangle - 1\right\}, \quad (5)$$

where $\mathbf{u}_{CH}(t)$ is the unit vector along the vector under study at time t. The calculated data indicate that there is a large deviation in the decorrelation rate of different vectors defined by atoms of the cation and the anion. In all IL systems studied, the vectors defined by atoms close to the imidazolium ring, such as N1–N3 and N1–C6, were found to decorrelate much slower than vectors defined by atoms at the end of the cation's alkyl chain due to the greater flexibility of the alkyl chain compared with the bonds attached to the imidazolium ring. In the anion, the bond that connects atoms C42 and S2 also decorrelates much faster than the vector defined by atoms S1 and S2, as can be seen from the different rates with which their $P_2(t)$ function decays to zero (not shown here). This behaviour is observed in all three ILs under study. Temperature has a strong influence on the rates of decorrelation of all vectors. As the temperature increases there is a significant raise in the decorrelation rate of all vectors defined on the ions, even for the stiffest ones such as that defined by the N1 and N3 atoms of the imidazolium ring.

These observations can be quantified by calculating the mean decorrelation time τ_C of each vector under study, defined by integrating the $P_2(t)$ function, which can be described accurately by the modified Kohlrausch–Williams–Watts (mKWW) function [77]:

$$P_{mKWW}(t) = \alpha\exp\left[-\left(\frac{t}{\tau_0}\right)\right] + (1-\alpha)\exp\left[-\left(\frac{t}{\tau_{KWW}}\right)^{\beta}\right]. \quad (6)$$

The mKWW function consists of two terms. The first describes a fast exponential decay with amplitude α associated with small perturbations of torsion angles around skeletal bonds and with the bond and bond-angle bending vibrations of skeletal and pendent bonds around their equilibrium values, and characteristic time τ_0. The second term is a slower stretching exponential decay (KWW) associated with cooperative conformational transitions in the ions, with τ_{KWW} being the characteristic correlation time and β the stretching exponent. By fitting the MD data for $P_2(t)$ to the $P_{mKWW}(t)$ function, one can calculate the mean decorrelation time τ_C through the expression:

$$\tau_C = \int_0^\infty P_2(t)\mathrm{d}t = \int_0^\infty P_{mKWW}(t)\mathrm{d}t = \alpha\tau_0 + (1-\alpha)\tau_{KWW}\frac{1}{\beta}\Gamma\left(\frac{1}{\beta}\right). \quad (7)$$

The calculated time τ_C for various vectors in the ILs at each temperature are reported in Table 4. It is also quantitatively evident that vectors defined by atoms near the imidazolium ring are much stiffer than others defined by atoms at the end of the alkyl chain. This behavior is observed at all temperatures, but it is more intense at the two lower temperatures, 298.15 and

Table 4. Mean decorrelation time, τ_C, for various bond vectors defined on $[C_4mim^+][Tf_2N^-]$, $[C_8mim^+][Tf_2N^-]$ and $[C_{12}mim^+][Tf_2N^-]$, as calculated from the mKWW fit to the $P_2(t)$ data.

	τ_C (ns)				
Bond vector	298.15 K	348.15 K	398.15 K	448.15 K	498.15 K
$[C_4mim^+][Tf_2N^-]$					
N1–N3	127.2	6.44	1.61	0.69	0.38
N3–C7	481.2	5.72	1.42	0.62	0.34
C9–C10	10.25	0.55	0.17	0.062	0.035
S1–S2	40.25	4.32	1.08	0.44	0.27
$[C_8mim^+][Tf_2N^-]$					
N1–N3	984.2	9.07	2.09	0.82	0.50
N3–C7	86.74	6.67	2.01	0.78	0.47
C13–C14	4.23	0.68	0.18	0.071	0.040
S1–S2	15.43	2.92	0.78	0.35	0.20
$[C_{12}mim^+][Tf_2N^-]$					
N1–N3	304770	38.58	4.79	1.55	0.80
N3–C7	247.4	15.87	4.61	1.49	0.75
C17–C18	11.11	1.81	0.29	0.091	0.044
S1–S2	61.99	6.89	1.85	0.70	0.35

348.15 K. In Figure 9 the τ_C for various vectors defined by atoms on $[C_{12}mim^+][Tf_2N^-]$ are presented on a logarithmic scale versus the inverse of the temperature. Figure 9 clearly demonstrates the wide range of relaxation times that characterize the segmental dynamics of these ILs, especially at the lowest temperature.

Additionally, the torsional dynamics can be studied using the torsion autocorrelation function, defined as

$$P_\varphi(t) = \frac{\langle \cos(\varphi(t))\cos(\varphi(0))\rangle - \langle \cos(\varphi(0))\rangle^2}{\langle \cos(\varphi(0))\cos(\varphi(0))\rangle - \langle \cos(\varphi(0))\rangle^2}, \quad (8)$$

where $\varphi(t)$ is the value of the torsion angle at time t. As expected from the analysis for the reorientation of the various vectors, torsions defined near the end of the cation's alkyl chain decorrelate much faster than those defined near the imidazolium ring. The $P_\varphi(t)$ data can also be represented by the mKWW function and the

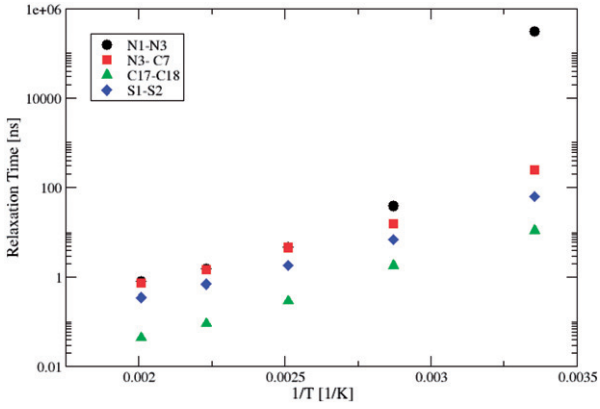

Figure 9. Relaxation times of vectors between atoms of the $[C_{12}mim^+][Tf_2N^-]$ IL, plotted on a logarithmic scale, as a function of the inverse temperature.

mean correlation time τ_C for the torsional motion can also be calculated from Equation (7). Table 5 reports the mean decorrelation times for torsions close to the imidazolium ring and at the end of the alkyl chain for the ILs. As expected, the mean decorrelation times reported for the torsion defined near the imidazolium ring are longer than those for the torsion defined by the terminal atoms of the alkyl chain. As the alkyl chain becomes longer the τ_C of the stiffest torsion, which is closer to the imidazolium ring, increases, in contrast to the last torsion of the alkyl tail that relaxes faster as the alkyl tail becomes longer. This is also obvious from the $P_\varphi(t)$ data shown in Figure 10. Temperature plays an important role in the torsion decorrelation rate: the higher the temperature the faster the torsional decorrelation rate, and therefore the mean decorrelation times decrease, as can be seen in Table 5. The timescale separation that governs the overall segmental dynamics of these ILs at low temperatures has been observed for ILs both in experimental and simulation studies and resembles the complex dynamical behaviour of polymeric systems [77–79].

3.4. *Self-diffusion coefficients*

ILs have much more complex dynamics than conventional fluids due to the different timescales that are involved in the local dynamics, as shown in the previous section. The self-diffusivity of the ions can be calculated by the Einstein relation:

$$D = \frac{1}{6}\lim_{t\to\infty}\frac{d}{dt}\langle|\mathbf{r}_i(t) - \mathbf{r}_i(0)|^2\rangle, \quad (9)$$

where $\mathbf{r}_i(t)$ is the position of the ith ion's center of mass at time t and the brackets denote the mean-square displacement (MSD) over the ions' centers of mass. Equation (9) is valid only when the diffusivity is in the

Table 5. Mean decorrelation time, τ_C, for various torsion angles defined on $[C_4mim^+][Tf_2N^-]$, $[C_8mim^+][Tf_2N^-]$ and $[C_{12}mim^+][Tf_2N^-]$, as calculated from the mKWW fit to the $P_\varphi(t)$ data.

	τ_C (ns)				
Torsion angle	298.15 K	348.15 K	398.15 K	448.15 K	498.15 K
$[C_4mim^+][Tf_2N^-]$					
N3–C7–C8–C9	2.16	0.53	0.17	0.079	0.051
C7–C8–C9–C10	2.39	0.32	0.12	0.067	0.043
$[C_8mim^+][Tf_2N^-]$					
N3–C7–C8–C9	17.68	1.08	0.37	0.18	0.11
C11–C12–C13–C14	0.99	0.26	0.12	0.074	0.073
$[C_{12}mim^+][Tf_2N^-]$					
N3–C7–C8–C9	26.05	3.21	0.72	0.36	0.16
C15–C16–C17–C18	1.54	0.26	0.13	0.063	0.041

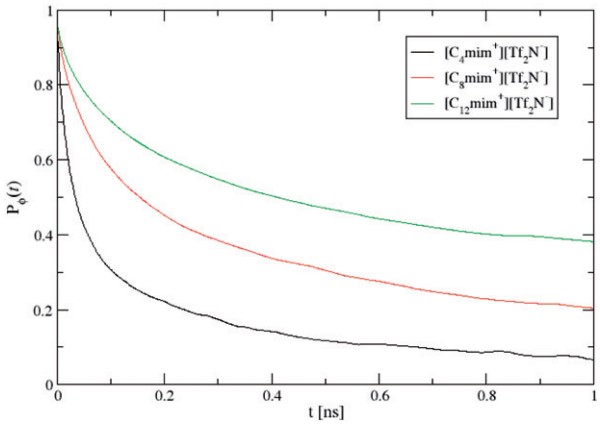

Figure 10. The $P_\varphi(t)$ function for the decorrelation of the torsion defined by the atoms N3–C7–C8–C9 of $[C_4mim^+][Tf_2N^-]$, $[C_8mim^+][Tf_2N^-]$ and $[C_{12}mim^+][Tf_2N^-]$ at 298.15 K and 1 bar.

Fickian regime, which can be identified by the slope being equal to unity in a log(MSD) versus log(t) plot. ILs have been found to have very sluggish dynamics compared with conventional fluids, especially at low temperatures where the Fickian regime is difficult to reach. At short times where ballistic motion is observed, the slope is greater than unity, while at intermediate times ILs exhibit glass-like behavior and the slope in that regime is less than one.

The calculated diffusivities for the three ILs, $[C_4mim^+][Tf_2N^-]$, $[C_8mim^+][Tf_2N^-]$ and $[C_{12}mim^+][Tf_2N^-]$, are shown in Figures 11(a), (b) and (c), respectively, as a function of temperature. Additionally, the experimental measurements [16] for both $[C_4mim^+][Tf_2N^-]$ and $[C_8mim^+][Tf_2N^-]$ in the temperature range 263–353 K are also shown. The cation self-diffusion coefficients are larger than those of the anion for $[C_4mim^+][Tf_2N^-]$ and $[C_8mim^+][Tf_2N^-]$ at all temperatures, a fact that has already been reported for most imidazolium-based ILs both from experiment [40,41] and simulation [1,44,80–83]. The increase of the alkyl chain length leads to reduced cation mobility and to smaller differences in the self-diffusivities of the anion and the cation so that, in the case of $[C_{12}mim^+][Tf_2N^-]$, the two ions have comparable self-diffusion coefficients. The self-diffusion coefficients calculated from MD were underestimated compared with the experimental values [16] for $[C_4mim^+][Tf_2N^-]$ and $[C_8mim^+][Tf_2N^-]$ at low temperatures, a problem that is generally reported in most molecular simulation studies [1,66,82,84]. No experimental data were available for higher temperatures for these two ILs and for $[C_{12}mim^+][Tf_2N^-]$ at all temperatures. Admittedly, there is a discrepancy between the results presented here for $[C_4mim^+][Tf_2N^-]$ and $[C_8mim^+][Tf_2N^-]$ at 298 K and those reported in Ref. [43] for the self-diffusion coefficients. Recent analysis of the raw simulation data of Ref. [43] revealed several technical problems in the simulation process and consequently, the self-diffusion coefficient values reported in Ref. [43]

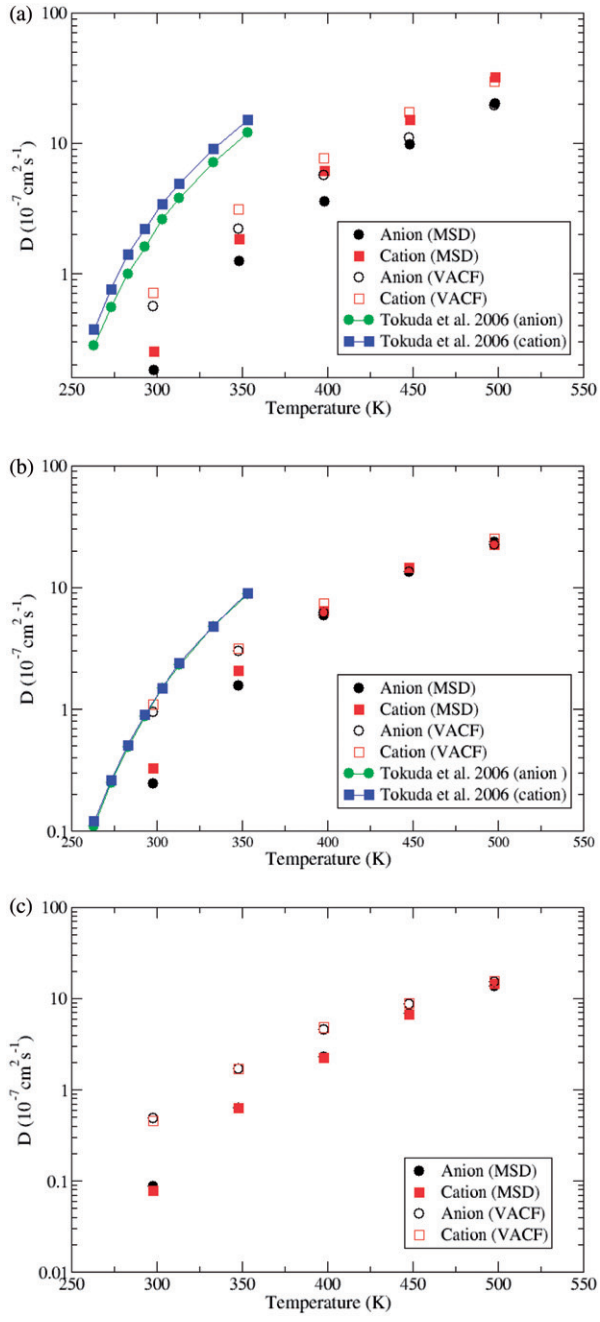

Figure 11. Self-diffusion coefficients of (a) $[C_4mim^+][Tf_2N^-]$, (b) $[C_8mim^+][Tf_2N^-]$ and (c) $[C_{12}mim^+][Tf_2N^-]$ as calculated by the Einstein (MSD) and Green–Kubo (VACF) expressions. The lines correspond to experimental measurements [16].

Table 6. Activation energies obtained from fitting an Arrhenius expression to the self-diffusivities calculated by the Einstein relation.

	Activation energy ($kJ\,mol^{-1}$)	
	E_{D-}	E_{D+}
$[C_4mim^+][Tf_2N^-]$	30.0	29.1
$[C_8mim^+][Tf_2N^-]$	28.9	28.3
$[C_{12}mim^+][Tf_2N^-]$	33.3	32.7

are problematic. Diffusion coefficient values using the force field of Ref. [43] are close to the values reported here for the same ILs.

The self-diffusion coefficients were also calculated using the Green–Kubo formula:

$$D = \frac{1}{3}\int_0^\infty \mathrm{d}t\langle \mathbf{v}_i(t)\cdot\mathbf{v}_i(0)\rangle, \tag{10}$$

where $\mathbf{v}_i(t)$ is the velocity of the center of mass of ion i at time t and the term inside the brackets is the velocity autocorrelation function (VACF). The self-diffusion coefficients were calculated using the last 2 ns of each trajectory with the information on velocity being stored every 10 fs. Although the two expressions (Equations (9) and (10)) for the calculation of diffusivity are in principle equivalent and are expected to give statistically indistinguishable results when applied to simple liquids, the Green–Kubo method is more prone to errors in cases of systems with complex local dynamics and modes of motion that take place in a wide range of timescales [1,82]. The self-diffusion coefficients obtained from the Green–Kubo method are systematically higher than those calculated using the Einstein relation (Figures 11(a), (b) and (c)), especially at low temperatures, a fact that has been presented in previous simulation studies for a number of ionic liquids [82,85–87]. Thus, even though Green–Kubo diffusivity coefficients appear to be closer to the experimental values at low temperatures, results obtained from the Einstein relation are considered more reliable [88]. The values obtained from the two methods for all ILs progressively converge as the temperature increases, since, at high temperatures, local dynamics decorrelate fast enough to be adequately sampled by the Green–Kubo method.

Diffusivity calculations using the Einstein relation were used to calculate the activation energies for diffusion shown in Table 6 by fitting to an Arrhenius expression. In all cases, the activation energy for the anion is greater than that of the cation, as expected from the values of the diffusivity obtained from the simulations, in agreement with activation energy calculations reported in the literature [9,10,82].

The fact that molecular simulation underestimates the diffusivity at low temperatures may be attributed to the fixed atomic charges that cause the formation of long-living cages in order to achieve charge neutrality among groups of ions, which results in a slower dynamics [52]. It has been proposed [53,56,57] that taking into account polarizability effects leads to better low-temperature self-diffusion predictions compared with experimental values. Moreover, strong dynamical heterogeneity has been observed in imidazolium-based ILs [51,52,83,89], which can be directly related to the spatial heterogeneity due to the tail aggregation phenomena. First results on the heterogeneity in the dynamics of the ILs under study [90] indicate that the low-temperature dynamics of these ILs is strongly heterogeneous, leading to the formation of individual clusters consisting of mobile or immobile ions inside the bulk. At high temperatures the heterogeneity in the dynamics appears mostly at very short times when the motion of the ions is ballistic. At time-scales that are relevant to the Fickian regime there is no evidence of heterogeneity in the dynamics, probably indicating that the high-temperature diffusivities calculated may be a more accurate estimation of the self-diffusivities of these systems.

3.5. *Shear viscosity*

Calculations of the shear viscosity were performed using the following Green–Kubo relation:

$$\eta = \frac{V}{k_B T}\int_0^\infty \mathrm{d}t\langle P_{ij}(t)\cdot P_{ij}(0)\rangle, \tag{11}$$

where $P_{ij}(t)$ is the ij-element of the pressure tensor at time t. The shear viscosity is a collective quantity and its calculation is prone to errors due to the sensitivity of the stress correlation function to the intramolecular vibrational modes. The stress correlation function was integrated at the last section of each productive run and the viscosity was estimated by the integral plateau value. In Figures 12(a), (b) and (c) the values for the viscosity for $[C_4mim^+][Tf_2N^-]$, $[C_8mim^+][Tf_2N^-]$ and $[C_{12}mim^+][Tf_2N^-]$, respectively, are plotted and compared with experimental data [15–17,91]. As expected, simulation overestimates the viscosity, being consistent with the slower dynamics that has been determined from the calculations of diffusivities, whereas the

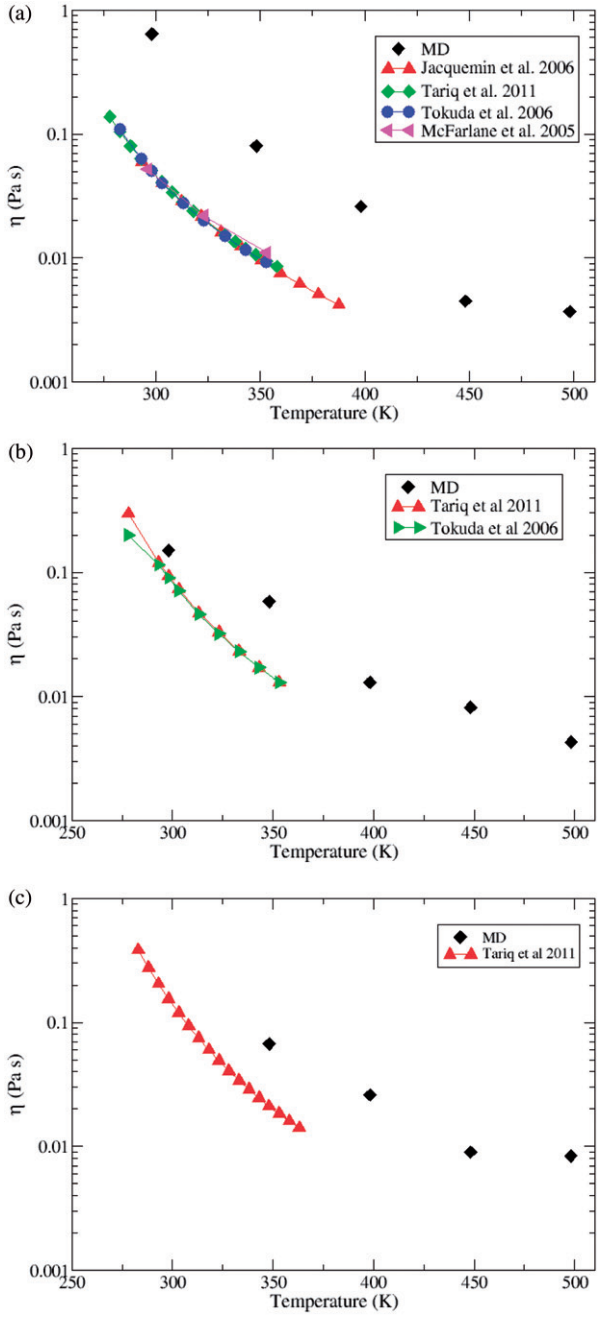

Figure 12. Shear viscosity MD results for (a) $[C_4mim^+][Tf_2N^-]$ (experimental values from Refs. [15–17,87]), (b) $[C_8mim^+][Tf_2N^-]$ (experimental values from Refs. [15,16]) and (c) $[C_{12}mim^+][Tf_2N^-]$ (experimental values from Ref. [15]). No value of the shear viscosity was included for $[C_{12}mim^+][Tf_2N^-]$ at 298.15 K as the integral of the pressure tensor autocorrelation function failed to reach a smooth plateau at that temperature.

temperature dependence of viscosity reproduces rather well the experimental results for all IL systems.

4. Conclusions

Long MD simulations of several tens of nanoseconds were performed over a wide temperature range from 298.15 to 498.15 K with 50 K increments and at atmospheric pressure in order to study the thermodynamic (density, thermal expansion, isothermal compressibility), structural (radial distribution functions between the centers of mass of ions and radial distribution functions between different sites of the ions, radial-angular distribution functions, end-to-end distance distributions) and dynamic (relaxation times in segmental dynamics, self-diffusion coefficients, shear viscosity) properties of imidazolium-based ILs, namely $[C_4mim^+][Tf_2N^-]$, $[C_8mim^+][Tf_2N^-]$ and $[C_{12}mim^+][Tf_2N^-]$. The temperature effect was thoroughly studied, as well as the influence of the cation's alkyl chain length on the properties under investigation.

The calculated radial and radial-angular distribution functions between the ions' centers of mass reveal that ILs exhibit organization at much longer distances than ordinary molecules with the anion–cation interaction being stronger than the other two interactions at all temperatures. There is a clear indication of alkyl tail aggregation, which becomes more evident for the longer alkyl chain lengths, while the anions were found to localize near the cation's imidazolium ring where the positive charge is located.

The dynamics of these ILs were found to be extremely sluggish, as indicated by the wide range of relaxation times that characterize their segmental dynamics, a fact that makes the calculation of their transport properties a very complicated task, especially at low temperatures, while the lack of experimental data at high temperatures hinders the verification of molecular simulation diffusivity predictions. However, molecular simulation results for viscosity were consistent with those for diffusivity and the temperature dependence of these properties was captured well.

A wealth of information on the microscopic mechanisms that govern the spatial organization and the dynamical behaviour of these systems was revealed, especially by the comparative study of the three IL systems with varying cation alkyl chain. Further improvement of existing force fields or the development of new ones that will incorporate the polarizability of the systems may increase the agreement between experimental data and simulations for the

transport properties of ionic liquids, especially at low temperatures.

Acknowledgement

The MD simulations were largely performed under the HPC-EUROPA2 project (project No. 228398) with the support of the European Commission – Capacities Area – Research Infrastructures. This work is part of the Project "THALIS" which is implemented under the Operational Project "Education and Life Long Learning" and is co-funded by the European Union (European Social Fund) and National Resources (ESPA).

Supporting Information Available: A complete list of the force field parameters used in this work is presented in Tables I to VI. Furthermore, representative calculations regarding the radial distribution function, the mean square displacement and the normalized velocity autocorrelation function for various ILs are shown in Figures S1 to S3, respectively.

References

[1] E.J. Maginn, J. Phys. Condens. Matter **21**, 373101 (2009).
[2] C.P. Fredlake, J.M. Crosthwaite, D.G. Hert, S.N.V.K. Aki and J.F. Brennecke, J. Chem. Eng. Data **49**, 954 (2004).
[3] K.N. Marsh, J.A. Boxall and R.L. Lichtenhaler, Fluid Phase Equilib. **219**, 93 (2004).
[4] T. Welton, J. Chem. Rev. **99**, 2071 (1999).
[5] H. Weingärtner, J. Angew. Chem Int. Ed. **47**, 654 (2008).
[6] B.S. Philipsa and J.S. Zabinskib, Trib. Lett. **17**, 555 (2004).
[7] T. Weidlich, M. Stočes and I. Švancara, in *Sensing in Electroanalysis*, edited by K. Vytřas, K. Kalcher, and I. Švancara (University Press Center, Parduice, Czech Republic, 2010).
[8] P. Wasserscheid and T. Welton, editors, *Ionic Liquids in Synthesis* (Wiley–VCH, Weinheim, Germany, 2003).
[9] H. Tokuda, K. Hayamizu, K. Ishii, Md.A.B.H. Susan and M. Watanabe, J. Phys. Chem. B **108**, 16593 (2004).
[10] H. Tokuda, K. Hayamizu, K. Ishii, Md.A.B.H. Susan and M. Watanabe, J. Phys. Chem. B **109**, 6103 (2005).
[11] S. Zhang, N. Sun, X. He, X. Lu and X. Zhang, J. Phys. Chem. Ref. Data **35**, 1475 (2006).
[12] E.W. Castner Jr and J.F. Wishart, J. Chem. Phys. **132**, 120901 (2010).
[13] R. Gomes de Azevedo, J.M.S.S. Esperança, J. Szydlowski, Z.P. Visak, P.F. Pires, H.J.R. Guedes and L.P.N. Rebelo, J. Chem. Thermodynam. **37**, 888 (2005).
[14] C. Hardacre, J.D. Holbrey, S.E.J. McMath, D.T. Bowron and A.K. Soper, J. Chem. Phys. **118**, 273 (2003).
[15] M. Tariq, P.J. Carvalho, J.A.P. Coutinho, I.M. Marrucho, L.N.C. Lopes and L.P.N. Rebelo, Fluid Phase Equilib. **301**, 22 (2011).
[16] H. Tokuda, S. Tsuzuki, M.A.B.H. Susan, K. Hayamizu and M. Watanabe, J. Phys. Chem. B **110**, 19593 (2006).
[17] J. Jacquemin, P. Husson, A.A. Padua and V. Majer, Green Chem. **8**, 172 (2006).
[18] J. Jacquemin, P. Husson, V. Majer and M.F. Costa Gomes, J. Solut. Chem. **36**, 967 (2007).
[19] J. Jacquemin, P. Husson, V. Mayer and I. Cibulka, J. Chem. Eng. Data **52**, 2204 (2007).
[20] R.L. Gardas, M.G. Freire, P.J. Garvalho, I.M. Marrucho, I.M.A. Fonsece, A.B.M. Ferreira and J.A.P. Countinho, J. Chem. Eng. Data **52**, 1881 (2007).
[21] A. Wandschneider, J.K. Lehmann and A. Heintz, J. Chem. Eng. Data **53**, 596 (2008).
[22] C.P. Fredlake, J.M. Crosthwaite, D.G. Hert, S.N.V.K. Aki and J.F. Brennecke, J. Chem. Eng. Data **49**, 954 (2004).
[23] M. Krummen, P. Wasserscheid and J. Gmehling, J. Chem. Eng. Data **47**, 1411 (2002).
[24] A. Heintz, D.V. Kulikov and S.P. Verekin, J. Chem. Eng. Data **47**, 894 (2002).
[25] J.M.S.S. Esperança, Z.P. Visak, N.V. Plechkova, K.R. Seddon, H.J.R. Guedes and L.P.N. Rebelo, J. Chem. Eng. Data **51**, 2009 (2006).
[26] J.G. Huddleston, A.E. Visser, W.M. Reichert, H.D. Willauer, G.A. Broker and R.D. Rogers, Green Chem. **3**, 156 (2001).
[27] B.D. Fitchett, T.N. Knepp and J.C. Conboy, J. Electrochem. Soc. **151**, E219 (2004).
[28] R. Kato and J. Gmehling, J. Chem. Thermodynam. **37**, 603 (2005).
[29] J. Kumelan, Á. Pérez-Salado Kamps, D. Tuma and G. Maurer, J. Chem. Thermodynam. **38**, 1396 (2006).
[30] A. Muhammad, M.I.A. Mutalib, C.D. Wilfred, T. Murugesan and A. Shafeeq, J. Chem. Thermodynam. **40**, 1433 (2008).
[31] J. Lachwa, P. Morgado, J.M.S.S. Esperança, H.J.R. Guedes, J.N.C. Lopes and L.P.N. Rebelo, J. Chem. Eng. Data **51**, 2215 (2006).
[32] J.A. Widegren and J.W. Magee, J. Chem. Eng. Data **52**, 2331 (2007).
[33] M.E. Kadil and K.N. Marsh, J. Chem. Eng. Data **52**, 2382 (2007).
[34] L. Alonso, A. Arce, M. Francisco and A. Soto, J. Chem. Eng. Data **52**, 2409 (2007).
[35] L. Alonso, A. Arce, M. Francisco and A. Soto, J. Chem. Eng. Data **53**, 1750 (2007).
[36] A.E. Andreatta, A. Arce, E. Rodil, A. Soto, L. Alonso, A. Arce, M. Francisco and A. Soto, J. Chem. Eng. Data **54**, 1022 (2009).
[37] L. Alonso, A. Arce, M. Francisco and A. Soto, J. Chem. Thermodynam. **40**, 265 (2008).
[38] D.H. Zaitsau, G.J. Kado, A.A. Strechan and Y.U. Paulechka, J. Phys. Chem. A **110**, 7303 (2006).

[39] L.I.N. Tomé, P.J. Carvalho, M.F. Freire, I.M. Marrucho, I.M.A. Fonseca, A.G.M. Ferreira, J.A.P. Coutinho and R.L. Gargas, J. Chem. Eng. Data **53**, 1914 (2008).

[40] T. Umecky, M. Kanakubo and Y. Ikushima, Fluid Phase Equilib. **228**, 329 (2005).

[41] M. Kanakubo, K.R. Harris, N. Tsuchihashi, K. Ibuki and M. Ueno, J. Phys. Chem. B **111**, 2062 (2007).

[42] J.N.A. Canongia Lopes and A.A.H. Pádua, J. Phys. Chem. B **110**, 3330 (2006).

[43] G. Logotheti, J. Ramos and I.G. Ecomomou, J. Phys. Chem. B **113**, 7211 (2009).

[44] T.I. Morrow and E.J. Maginn, J. Phys. Chem. B **106**, 12807 (2002).

[45] S.M. Urahata and M.C.C. Ribeiro, J. Chem. Phys. **120**, 1855 (2004).

[46] G. Raabe and J. Köhler, J. Chem. Phys. **128**, 154509 (2008).

[47] B. Qiao, C. Krekeler, R. Berger, L.D. Site and C. Holm, J. Phys. Chem. B **112**, 1743 (2008).

[48] J.N. Canongia Lopes, J. Deschamps and A.A.H. Pádua, J. Phys. Chem. B **108**, 2038 (2004).

[49] A.A.H. Pádua, M.F. Costa Gomes and J.N.A. Canongia Lopez, Acc. Chem. Res. **40**, 1087 (2007).

[50] Y. Wang and G.A. Voth, J. Am. Chem. Soc. **127**, 12192 (2005).

[51] Y. Wang and G.A. Voth, J. Phys. Chem. B **110**, 18601 (2006).

[52] Y. Wang, W. Jiang, T. Yan and G.A. Voth, Acc. Chem. Res. **40**, 1193 (2007).

[53] T. Yan, C.J. Burnham, M.G. Del Popolo and G.A. Voth, J. Phys. Chem. B **108**, 11877 (2004).

[54] Y. Wang, S. Izvenov, T. Yan and G.A. Voth, J. Phys. Chem. B **110**, 3564 (2006).

[55] H.I. Karimi-Varzaneh, F. Müller-Plate, S. Balasubramanian and P. Carbone, Phys. Chem. Chem. Phys. **12**, 4714 (2010).

[56] O. Borodin and G.D. Smith, J. Phys. Chem. B **110**, 11481 (2006).

[57] O. Borodin, J. Phys. Chem. B **113**, 11463 (2009).

[58] J.C. Phillips, R. Braun, W. Wang, J. Gumbart, E. Tajkhorshid, E. Villa, C. Chipot, R.D. Skeel, L. Kalé and K. Schulten, J. Comput. Chem. **26**, 1781 (2005).

[59] P.J. Flory, *Statistical Mechanics of Chain Molecules* (Wiley, New York, 1969).

[60] D.N. Theodorou and U.W. Suter, Macromolecules **18**, 1467 (1985).

[61] D.N. Theodorou and U.W. Suter, Macromolecules **19**, 139 (1986).

[62] More information can be found at www.scienomics.com

[63] M. Tuckerman, B.J. Berne and G.J. Martyna, J. Chem. Phys. **97**, 1990 (1992).

[64] G.J. Martyna, M.E. Tuckerman, D.J. Tobias and M.L. Klein, Mol. Phys. **87**, 1117 (1996).

[65] C. Cadena and E.J. Maginn, J. Phys. Chem. B **110**, 18026 (2006).

[66] C. Cadena, Q. Zhao, R.Q. Snurr and E.J. Maginn, J. Phys. Chem. B **110**, 2821 (2006).

[67] J.N. Canongia Lopes and A.A.H. Pádua, J. Phys. Chem. B **108**, 16893 (2004).

[68] J. de Andrade, E.S. Böes and H. Stassen, J. Phys. Chem. B **106**, 3546 (2002).

[69] S. Takahashi, K. Suzuya, K. Kohara, N. Koura, L.A. Curtiss and M.L.Z. Saboungi, Phys. Chem. (Munich) **209**, 209 (1999).

[70] C. Hardacre, S.E.J. McMath, M. Nieuwenhuyzen, D.T. Bowron and A.K. Soper, J. Phys. Condens. Matter **15**, S159 (2003).

[71] J.K. Shah, J.F. Brennecke and E.J. Maginn, Green Chem. **4**, 112 (2002).

[72] C.J. Margulis, H.A. Stern and B.J. Berne, J. Phys. Chem. B **106**, 12017 (2002).

[73] C.G. Hanke, S.L. Price and R.M. Lynden-Bell, Mol. Phys. **99**, 801 (2001).

[74] M.G. Del Popolo and G.A. Voth, J. Phys. Chem. B **108**, 1744 (2004).

[75] Z.A. Makrodimitri, D.J.M. Unruh and I.G. Economou, J. Phys. Chem. B **115**, 1429 (2011).

[76] M. Modello, G.S. Grest, E.B. Webb III and P. Peczak, J. Chem. Phys. **109**, 798 (1998).

[77] M. Doxastakis, D.N. Theodorou, G. Fytas, F. Kremer, R. Faller, F. Müller-Plathe and N. Hadjichristidis, J. Chem. Phys. **119**, 6883 (2003).

[78] G.E. Logotheti and D.N. Theodorou, Macromolecules **40**, 2235 (2007).

[79] V. Arrighi, D. Batt-Coutrot, C. Zhang, M.T.F. Telling and A. Triolo, J. Chem. Phys. **119**, 1271 (2003).

[80] Z. Liu, S. Huang and W. Wang, J. Phys. Chem. B **108**, 12978 (2004).

[81] T. Ködderman, D. Paschek and R. Ludwig, Chem. Phys. Chem. **8**, 2464 (2007).

[82] H. Liu and E. Maginn, J. Chem. Phys. **135**, 124507 (2011).

[83] S.M. Urahata and M.C.C. Ribeiro, J. Chem. Phys. **122**, 024511 (2005).

[84] A. Bagno, F. D'Amico and G. Saielli, J. Mol. Phys. **131/132**, 17 (2007).

[85] M.H. Kowsari, S. Alavi, M. Ashrafizaadeh and B. Najafi, J. Chem. Phys. **129**, 224508 (2008).

[86] M.H. Kowsari, S. Alavi, B. Najafi, K. Gholizadeh, E. Dehghanpieh and F. Ranjbar, Phys. Chem. Chem. Phys. **13**, 8826 (2011).

[87] C. Rey-Castro and L.F. Vega, J. Phys. Chem. B **110**, 14426 (2006).

[88] E.J. Maginn, Rev. Comput. Chem. **26**, 421 (2009).

[89] T. Ködderman, D. Paschek and R. Ludwig, Chem. Phys. Chem. **9**, 1851 (2008).

[90] E. Androulaki, N. Vergadou and I.G. Economou, in preparation.

[91] J. McFarlane, W.B. Ridenour, H. Luo, R.D. Hunt and D.W. De Paoli, Sep. Sci. Tech. **40**, 1245 (2005).